SOLVENT-CAST DIRECT-WRITE MICROFABRICATION OF THERMOPLASTIC-BASED NANOCOMPOSITE STRUCTURES

S.Z. Guo[1], M-C Heuzey[2] and D. Therriault[1]*
[1] Laboratory for Multiscale Mechanics
Center for applied research on polymers (CREPEC),
École Polytechnique de Montréal, Montréal (QC), Canada
[2] Chemical Engineering Department,
Center for applied research on polymers (CREPEC),
École Polytechnique de Montréal, Montréal (QC), Canada
* Corresponding author (daniel.therriault@polymtl.ca)

Keywords: *Microfabrication, Solvent-cast, Thermoplastics, Polylactide, Direct write*

1 Introduction

Direct-write (DW) assembly is a three-dimensional (3D) printing technique that employs a computer-controlled translation stage, which moves an ink-deposition nozzle, to create materials with the desired architecture and composition [1]. Many ink materials have been employed such as organic fugitive inks [2], concentrated polyelectrolyte complexes [3], colloidal suspensions [4], hydrogels [5] and thermoset polymers [6]. These inks solidify through different mechanisms such as viscoelastic recoil [2], coagulation in reservoir [3], suppression of repulsive forces [7], and UV polymerization [6]. UV curable epoxy/carbon nanotube nanocomposite was used to fabricate 3D freestanding sensors by the direct-write technique [6].

Polylactide (PLA) is one important material since it is thermoplastic, biodegradable, biocompatible and has a relative high-strength, high-modulus and good processability [8]. PLA can be prepared either by the polycondensation of lactic acid or by the ring opening polymerization of lactide [9]. Currently, the majority of lactic acid production is obtained from the fermentation of renewable sugar feedstock such as corn and sugar beets. Because of its low toxicity [10] and environmentally benign characteristics [11], PLA is becoming an ideal material for food packaging and for other consumer products [12]. In order to extend the range of applications, nanofillers (e.g. nanoclay, carbon nanotube) are used to improve the PLA properties including mechanical, fire retardant, rheological, gas barrier, and optical properties. P. Krishnamachari *et al.* studied the effects of nanoclay loading on the morphological, thermal and mechanical properties of PLA/nanoclay composites prepared by melt compounding with a twin screw extruder [13]. M. Pluta *et al.* investigated the dielectric properties of polylactide/clay nanocomposites [14]. Effect of nanoclay type on tensile, water vapor barrier and antimicrobial properties of PLA/nanoclay composites films prepared using a solvent casting method were reported by J. Rhim *et al* [15].

Thermoplastic polymers melts have been used in the fused deposition method because of their rigidity increase after the temperature-triggered phase transition from melt to solid [16]. However this method exhibits limited precision of the printed features and the high viscosity of most polymer melts may prevent the application of this technique to functional nanocomposite devices, since nanoparticles can significantly increase material viscosity. In addition, other methods including the surface tension driven direct-write [17] and soft lithographic approaches [18] were reported to fabricate 3D PLA scaffolds for tissue engineering. However, these methods are unable to build freeform 3D structures.

In this work, PLA, with and without nanoparticles, was used in the solution state to fabricate microstructures at room temperature in a freeform fashion by solvent-cast direct-write assembly (SC-DW) (Fig. 1.). The process apparent viscosity of the inks and their flow behavior were characterized using capillary flow analysis. Besides, the solvent evaporation rate of the inks after extrusion from the micro-nozzle was investigated. In addition, dynamic

mechanical analysis (DMA) using a film tension clamp was performed for the nanocomposite filaments featuring different nanoclay contents, or fabricated under different applied pressures and nozzle diameters. Moreover, the morphology of the geometries was examined by scanning electron microscopy (SEM). The information gathered here aims at elucidating the effects of process parameters on the properties of extruded micro-structures.

2 Experimental Methods

2.1 Materials

Semi-crystalline PLA (grade 4032D), manufactured by Natureworks LLC, was used as the matrix materials in this study. Organically treated montmorillonite Cloisite® 30B from Southern Clay Products was used as the nanofiller. This organoclay contains methyl-bis(2-hydroxy-ethyl) tallowalky ammonium cations [14]. A composite master batch with 20 wt% nanoclay loading was prepared by mixing PLA and nanoclay using twin-screw extruder in NRC-IMI laboratory. Various amounts of the master batch nanocomposite and neat PLA were dissolved in the solvent dichloromethane (DCM, Sigma-Aldrich) to prepare 20, 25 and 30 wt% solutions with the desired nanoclay loading in the composites (0, 0.5, 1, 1.5, 2, 5, 10 and 15 wt%).

2.2 Structure Fabrication

The PLA/nanoclay composite 2D and 3D structures were fabricated by the SC-DW technique. The deposition system consists of a computer controlled robot (I&J2200-4, I&J Fisnar) moving a dispensing apparatus (HP-7X, EFD) along the *x*, *y* and *z* directions (Fig. 1.). Under applied pressure, the polymer solution, which undergoes capillary shear flow inside the micro-nozzle, relaxes its stresses upon exiting the nozzle. As the solvent evaporates post extrusion, the diameter of the filament decreases and its rigidity gradually increases with time due to a locally higher polymer concentration. This rigidity gradient enables the creation of self-supporting curved shapes by changing the moving path of the extrusion nozzle, in which the filament bending occurs in the low rigidity zone of the newly extruded material. After most of the solvent evaporates, the rigidity of the extruded filament changes from fluid-like to solid-like, which facilitates the shape retention of the deposited features.

2.3 Morphological Characterization

The morphology of the various micro-structures was observed using a Jeol JSM-840 Scanning Electron Microscope (SEM). Samples were sputtered with gold for 15 s before the tests. The optical micrographs were captured using an Olympus SZX 12 stereomicroscope equipped with an Evolution VF color camera and analyzed with the image processing software Image-Pro Plus 6.0.

2.4 Capillary Flow Analysis

The process apparent viscosities of 25 wt% nanocomposite solutions with various nanoclay loadings (0, 0.5, 1, 1.5, 2, 5, 10 wt%) were calculated from constant-pressure capillary flow analysis as described in [19]. The ink was extruded through two different micro-nozzles (inner diameter

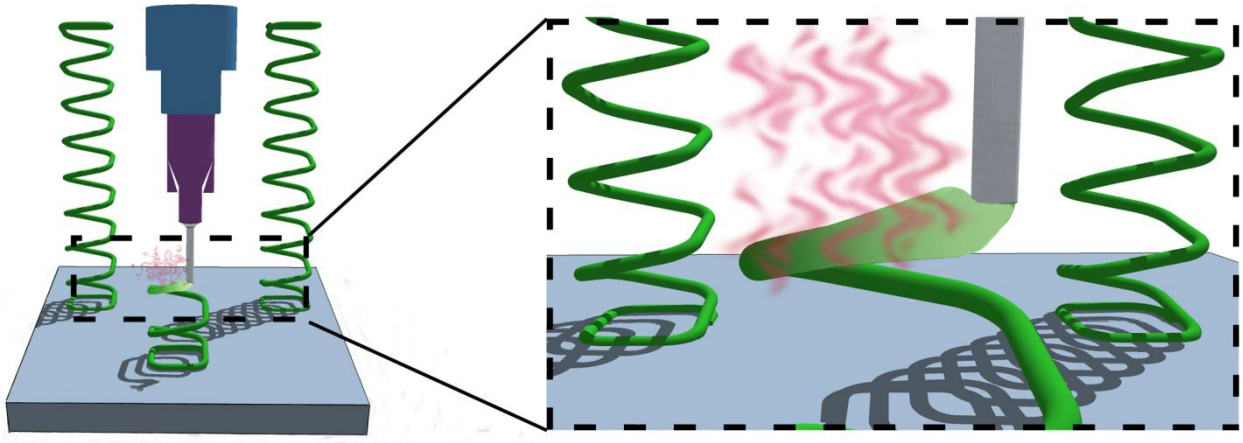

Fig. 1. Schematic of the SC-DW process with a thermoplastic solution. After extrusion from nozzle, the rigidity of the filament changes from fluid-like to solid-like due to fast solvent evaporation, this facilitates the shape retention of the deposited features.

= 100 and 200 μm). The high-capacity pressure dispenser was set between 400 and 3000 kPa depending on the nozzle diameter and the nanoclay loading. After reaching the extrusion steady state, the ink was deposited onto a substrate for 60 s under the various applied pressure at a robot velocity of 1 mm s^{-1} and repeated three times. After drying in the vacuum oven at 50 ℃ for 12 h, the extruded fibers were then weighted with a high precision balance (GH-202, A&D Engineering Inc., Milpitas, CA) to determine the mass flow rate, which was converted to the volumetric flow rate using the respective densities. Capillary data reported in this work include the Rabinowitch correction.

2.5 Solvent Evaporation Tests

The solvent evaporation behavior of the polymer inks was evaluated by directly depositing a filament with a 5 mm length on a glass substrate resting on a high-precision balance (GH-202, A&D Engineering Inc.). The computer controlled robot (I&J2200-4, I&J Fisnar) was used to deposit the three polymer solutions (20， 25 and 30 wt%) on the substrates for 5 s through a nozzle with a 510 μm (5121-0.25-B, EFD) inner diameter, under an applied pressure of 420 kPa. The 20 wt% PLA solution was also deposited through two other nozzles (inner diameter = 330 and 200 μm). The sample weight change was recorded for 6 h. Following this recording period, the sample was completely dried in an oven (G05053-10, Cole-Parmer) at 50 ℃ for 12 h and weighed again. The mass of the dried PLA was then used to calculate the solvent percentage in the deposited filament.

2.6 Mechanical Characterization

The specimens for the mechanical tests consisted of three parallel fibers (diameter of 60 μm) which were deposited on two PLA arrays, using the 25 wt% PLA solution with and without nanoclay (Cloisite® 30B) (Fig. 6.(a) inset). Before test, all the specimens were dried in vacuum oven at 50 ℃ for 12 h, then the samples were characterized using a DMA Q800 (TA instruments) for quasi-static tensile stress-strain test. After fixing the specimen in the tension clamps, two fibers were cut and one fiber was left for the test. The loading rate was set at 0.5 N min^{-1} and maintained until the fiber rupture.

3 Results and Discussions

3.1 Capillary Flow Analysis

Similar to the polymer solution electrospinning process [20], the direct ink writing technique with nanocomposite solution is influenced by the solution viscosity, and the solvent evaporation rate. It is desirable to estimate the apparent viscosity from the actual process data of capillary flow in the nozzle. The correlations between deposition parameters such as applied pressure, nozzle diameter (D), flow rate, and robot velocity (V) can be found by the capillary flow analysis. The results may guide the ink design and the adjustment of the deposition parameters. Fig. 2. shows the flow curves obtained by measuring the volumetric flow rate with respect to the applied pressure. For all nanocomposite solutions, the flow rate increased with the applied pressure. Under the same pressure, the flow rates of the nanocomposite solutions with nanoclay content below 1 wt% had a minor difference between each other, while

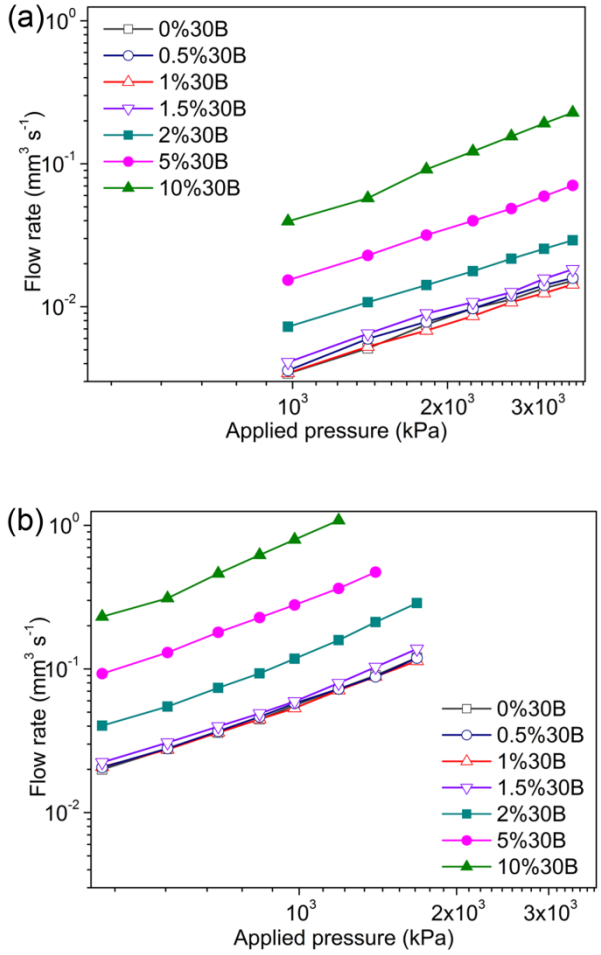

Fig. 2. The volumetric flow rate as a function of the applied pressure for different nanoclay loading composite solution. (composite concentration: 25wt%; V = 1mm s^{-1}; D = (a) 100 μm, (b) 200 μm.)

obviously increased as nanoclay loading increasing above 1.5 wt%. Similar finding were observed for the two nozzle diameters investigated (*i.e.*, 100 and 200 μm)

Because the ratio of micro nozzle length (L) to diameter (D) is larger than 50, the end effects in the capillary flow (or Bagley correction) can be ignored [21]. The process-related wall shear stress τ_w is calculated using the following equation:

$$\tau_w = \frac{P_{appl}}{2(L/R)} \quad (1)$$

where P_{appl} is the applied pressure during the process. The wall shear rate $\dot{\gamma}_w$ is determined from the volumetric flow rate Q, by calculating first the Newtonian shear rate $\dot{\gamma}_{Newt}$:

$$\dot{\gamma}_{Newt} = \frac{4Q}{\pi R^3} \quad (2)$$

and correcting for non-Newtonian effects using

$$\dot{\gamma}_w = \dot{\gamma}_{Newt}\left(\frac{3+b}{4}\right) \quad (3)$$

where the bracketed term is called the Rabinowitch correction. The parameter b, of the inverse of the power-law index n, is obtained from the log-log plot of τ_w with respect to $\dot{\gamma}_{Newt}$:

$$b = \frac{1}{n} = \frac{d\log(\dot{\gamma}_w)}{d\log(\tau_w)} \quad (4)$$

Finally, with Equation (3) representing the process-related shear rate, we can calculate the process

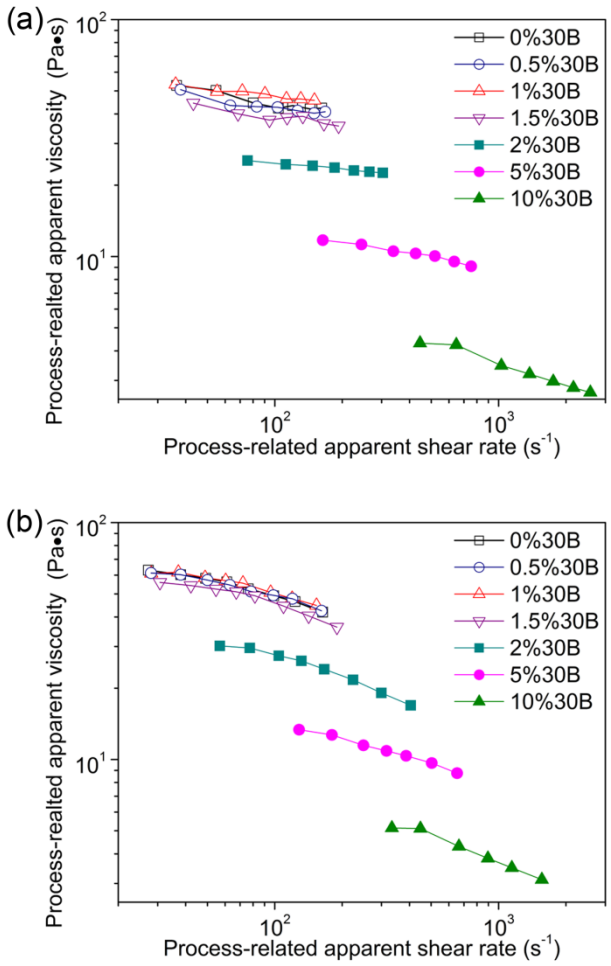

Fig. 3. Variation of the process-related apparent viscosity as a function of the apparent shear rate for different nanoclay loading composite solutions. (composite concentration: 25wt%; V = 1 mm s^{-1}; D = (a) 100μm, (b) 200μm.)

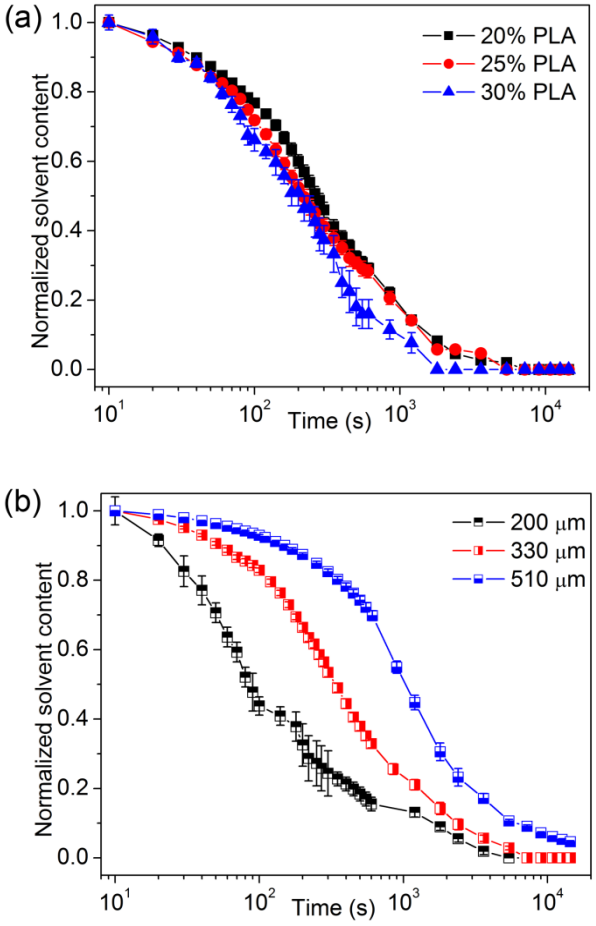

Fig. 4. Normalized solvent content as a function of time. (a) three PLA solutions deposited using 510 μm nozzle under 0.42 MPa applied pressure and 1 mm s^{-1} robot velocity for 5 seconds, and (b) 20 wt% PLA solution deposited using three nozzles under 0.42 MPa applied pressure and 1 mm s^{-1} robot velocity for 5 seconds.

apparent viscosity:

$$\eta_{app} = \frac{\tau_w}{\dot{\gamma}_W} \quad (5)$$

Fig. 3. presents the process apparent viscosity as a function of the process-related shear rate $\dot{\gamma}_w$ for different nanoclay loadings and micro nozzle diameters. All the solutions had a shear-thinning behavior within the range of shear rates studied here. The dynamic complex viscosity of melt nanocomposite was reported to be an increasing function of nanoclay content [22-24]. Here, the apparent viscosities of the composite solutions show no obvious differences when the nanoclay loadings are below 1wt%, however, it decrease significantly as for nanoclay loadings above 1.5 wt%. This reduction is most probably explained by the fact that the polymer content decrease as the nanoclay loading increases, since the overall concentration of the nanocomposite in the solution was kept constant. Comparing the Fig. 3. (a) and (b), nozzle diameter had no obvious effect on the nanocomposite solution rheological properties within the range studied.

3.2 Solvent Evaporation Rate

After filament extrusion from the micro-nozzle, the solvent evaporation plays a crucial role in the geometric retention, which is similar to the dry spinning process [25-27]. There are three mechanisms of solvent removal from the extruded filament: 1) flash vaporization, 2) diffusion within the filament, and 3) convective transfer from the filament surface to the surrounding air. Flash vaporization takes place near the nozzle tip due to a high pressure difference after the filament extrusion. Afterwards, the solvent molecules must first move through the filament (internal diffusion) and then evaporate at the air/filament interface (external convection). The solvent evaporation behavior was investigated by monitoring the weight reduction of the deposited filament as a function of time using a high-precision balance. Fig. 4.(a) shows the

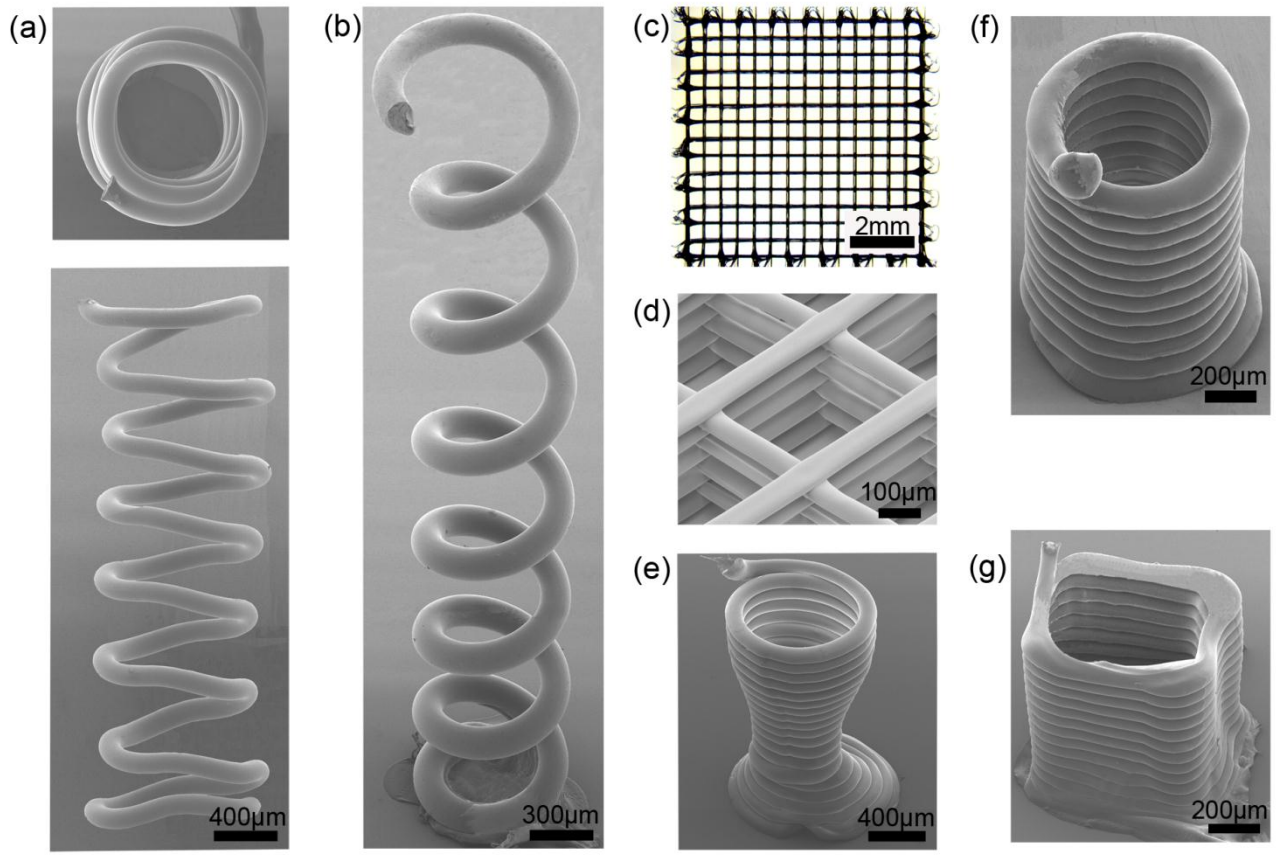

Fig. 5. Morphology of the microstructures. Representative SEM image of (a) top and side view of a PLA square spiral, (b) top view of a PLA circular spiral, (c) Representative optical image of a PLA scaffold composed of nine layers. (d) Inclined top view SEM image of PLA 9-layer scaffold. (e) SEM image of a PLA cup. (f) SEM image of a PLA circular tower. (g) SEM image of a PLA square tower.

normalized solvent content evolution with time for a short filament (length of ~5 mm) deposited using different neat PLA (20, 25 and 30 wt%) solutions through a 510 μm inner diameter nozzle. Since the data was recorded after the balance was stable, the stage of flash vaporization is not shown in the plots. For the filaments extruded using different PLA solutions, the plots of normalized solvent content versus time had no distinct difference. In other words, the initial solvent contents had no obvious effects on the solvent internal diffusion, which was also shown by N. Kojić *et al* [28]. Fig. 4.(b) displays similar plots for filaments extruded using the 20 wt% PLA solution through different nozzle diameters (200, 330 and 510 μm). The solvent evaporation rate intensely increased as the filament diameter decreased. This might be attributed to the fact that the solvent internal diffusion was greatly improved by shortening the diffusion distance. From the results shown in Fig. 4., it seems that the internal diffusion of the solvent through the filament is the governing process in the solvent removal of the extruded filaments.

3.3 Micro-structure Fabrication

Different kinds of 3D microstructures were fabricated by the SC-DW assembly including a square spiral, circular spiral, micro-cup, 9-layer scaffold and tower showed in Fig. 5 (a-g). This flexible method enabled the fabrication of unique structures that are generally difficult to produce by conventional single-stage processing methods, including floating (Fig. 5.(a) and (b)), spanning (Fig. 5. (c) and (d)) and scalable (Fig. 5.(e)) structures.

Fig. 5.(a) shows SEM top and side view images of the square spiral, which was fabricated with the 30 wt% PLA solution using a micro-nozzle with a 100 μm inner diameter under an applied pressure of 1.75 MPa and 0.1 mm s^{-1} robot velocity. For the circular spiral of Fig. 5.(b), the average spring diameter was 966±6 μm and the average pitch was 530±25 μm. Both values were very close to the programmed deposition path. The layer-by-layer scaffold (Fig. 5.(c, d)) and the micro-cup (Fig.5.(e)) were fabricated with the 25 wt% PLA solution using a 100 μm inner diameter nozzle under an applied pressure of 1.4 MPa and 1.0 mm s^{-1} robot velocity. The scaffold was almost identical to its programmed deposition paths because the printing layer was supported by the underlying layer. Fig. 5.(f) shows a circular tower with 1.0 mm diameter and 1.5 mm height, which was built with the 25 wt% PLA solution using a nozzle with a 100 μm inner diameter under an applied pressure of 1.05 MPa and 0.2 mm s^{-1} robot velocity. Fig. 5.(g) indicates a square tower with 1.0 mm side length and 1.5 mm

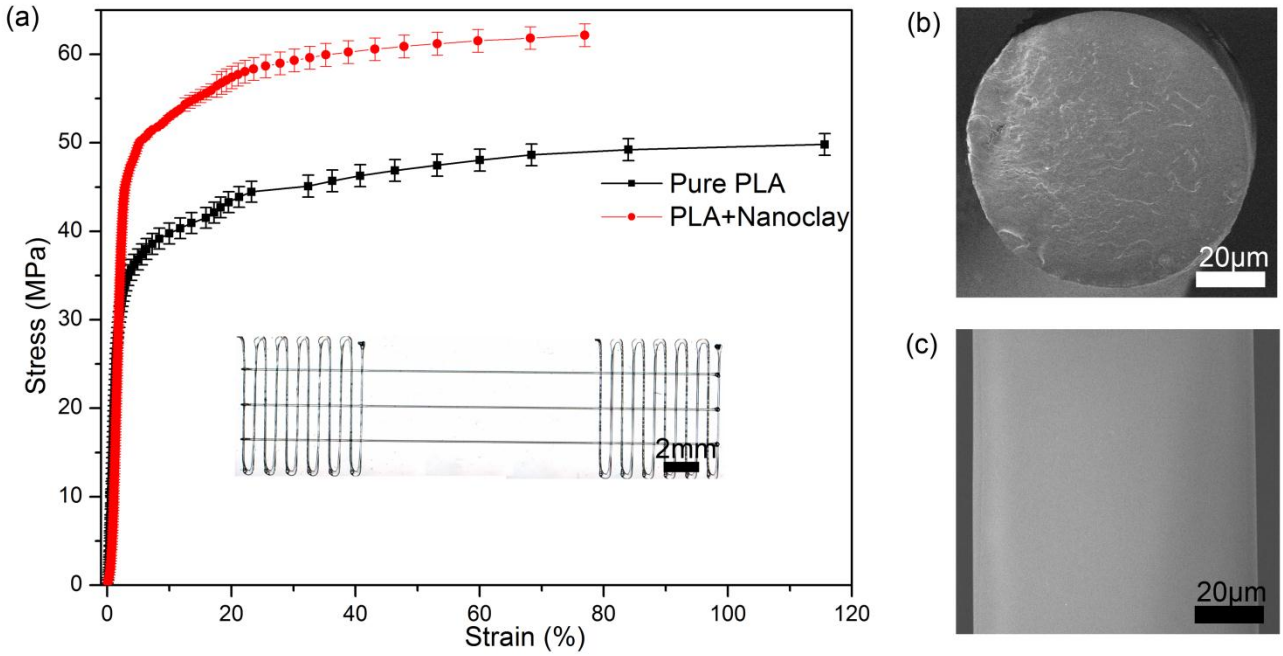

Fig. 6. PLA fiber specimen and mechanical characterization. a) Filament mechanical response under tensile loading, and the inset is an optical microscope image of the specimen for the mechanical characterization. b) Representative SEM image of the PLA filament circular cross section. c) Representative SEM image of the filament smooth surface.

height, which was produced using the same parameters as the circular tower. Consequently, the solvent-cast printing method is demonstrated to be a flexible and high fidelity micromanufacturing process for thermoplastic polymers.

3.4 Mechanical Properties

The measured stress-strain curves of PLA and its nanocomposite (1.5 wt% of Cloisite® 30B) microfibers are shown in Fig. 6. The Young's modulus and tensile strength for the nanocomposite are 2.42 GPa and 62 MPa, respectively, while the values for neat PLA are 2.05 GPa and 50 MPa. These results reveal that the mechanical properties are improved by dispersing a small amount of nanoclay in the polymer matrix due to the large surface area of layered silicate layers exposed to the polymer [29].

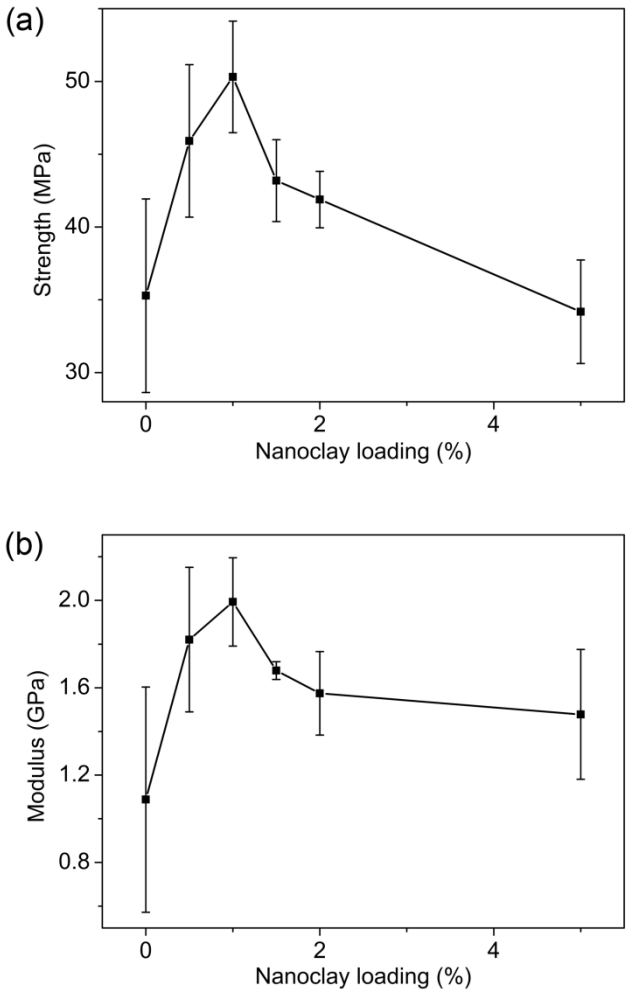

Fig. 7. Averaged mechanical properties measurement of (a) Modulus, (b) Strength for various nanoclay loadings.

J.-H. Chang, *et al.* reported that the tensile modulus and tensile strengths of PLA/nanoclay composite increased by 60% with nanoclay content and possessed a maximum value for a critical clay loading (2 - 4 wt% for three different nanoclays). Above this critical loading, the modulus and strength values of the nanocomposite started to decrease [30]. Here, a similar trend happened for the DMA tests on the PLA nanocomposite. Fig. 7. (a) and (b) show the average modulus and strength as functions of the nanoclay loading. The averaged DMA results come from three repetitions for each experiment and the error bar represents the 95% confidence interval. The critical loading is 1.0 wt%, at which the modulus increases by 83% and tensile strength increases by 43%. Higher nanoclay content will lead to a decreasing for both of the modulus and tensile strength.

Thermoplastic nanocomposites made with other types of nanoparticles such as carbon nanotube, graphene are assumed to be also compatible with the SC-DW method to fabricate 2D or 3D microstructures. These structures may exhibit multifunctional properties such as improved thermal and electrical conductivities, water and oxygen barriers, and magnetic shielding.

4 Conclusions

The SC-DW microfabrication technique developed here enables the facile room temperature printing of self-supporting and other types of thermoplastic polymers microstructures (e.g., conformal, layer-by-layer). The solution rheology can be tailored to facilitate both flow through fine deposition nozzles and solidification in air upon exiting the nozzle. The capillary flow analysis showed the polymer solutions were shear-thinning fluids, as expected. The modulus of PLA nanocomposite filaments can be enhanced by 83% at a critical nanoclay loading of 1.0 wt%. We believe that the compatibility of this process with thermoplastic-based nanocomposites materials will create new prospects for the micromanufacturing of complex 3D functional structures. This process could be used to create flexible electrical connections, freestanding strain sensors, or inductance components in organic microelectronics, as well as micro-prosthetic devices or tissue engineering scaffolds.

Acknowledgments

The authors acknowledge the financial support from NSERC (Natural Sciences and Engineering Research Council of Canada). A scholarship for Mr. Guo was also provided by the China Scholarship Council (CSC).

References

[1] J. A. Lewis and G. M. Gratson "Direct writing in three dimensions". *Materials Today*, Vol. 7, No. 7–8, pp. 32-39, 2004.

[2] D. Therriault, R. F. Shepherd, S. R. White, and J. A. Lewis "Fugitive Inks for Direct-Write Assembly of Three-Dimensional Microvascular Networks". *Advanced Materials*, Vol. 17, No. 4, pp. 395-99, 2005.

[3] G. M. Gratson, M. Xu, and J. A. Lewis "Microperiodic structures: Direct writing of three-dimensional webs". *nature*, Vol. 428, No. 6981, pp. 386-86, 2004.

[4] J. J. Adams, E. B. Duoss, T. F. Malkowski, M. J. Motala, B. Y. Ahn, R. G. Nuzzo, J. T. Bernhard, and J. A. Lewis "Conformal Printing of Electrically Small Antennas on Three-Dimensional Surfaces". *Advanced Materials*, Vol. 23, No. 11, pp. 1335-40, 2011.

[5] J. N. Hanson Shepherd, S. T. Parker, R. F. Shepherd, M. U. Gillette, J. A. Lewis, and R. G. Nuzzo "3D Microperiodic Hydrogel Scaffolds for Robust Neuronal Cultures". *Advanced Functional Materials*, Vol. 21, No. 1, pp. 47-54, 2011.

[6] R. D. Farahani, H. Dalir, V. L. Borgne, L. A. Gautier, M. A. E. Khakani, M. Lévesque, and D. Therriault "Direct-write fabrication of freestanding nanocomposite strain sensors". *Nanotechnology*, Vol. 23, No. 8, p. 085502, 2012.

[7] J. E. Smay, G. M. Gratson, R. F. Shepherd, J. Cesarano, and J. A. Lewis "Directed Colloidal Assembly of 3D Periodic Structures". *Advanced Materials*, Vol. 14, No. 18, pp. 1279-83, 2002.

[8] R. E. Drumright, P. R. Gruber, and D. E. Henton "Polylactic Acid Technology". *Advanced Materials*, Vol. 12, No. 23, pp. 1841-46, 2000.

[9] L. T. Lim, R. Auras, and M. Rubino "Processing technologies for poly(lactic acid)". *Progress in Polymer Science*, Vol. 33, No. 8, pp. 820-52, 2008.

[10] R. E. Conn, J. J. Kolstad, J. F. Borzelleca, D. S. Dixler, L. J. Filer Jr, B. N. Ladu Jr, and M. W. Pariza "Safety assessment of polylactide (PLA) for use as a food-contact polymer". *Food and Chemical Toxicology*, Vol. 33, No. 4, pp. 273-83, 1995.

[11] C. Danyluk, R. Erickson, S. Burrows, and R. Auras "Industrial Composting of Poly(Lactic Acid) Bottles". *Journal of Testing and Evaluation*, Vol. 38, No. 6, p. 7, 2010.

[12] J. Ahmed and S. K. Varshney "Polylactides—Chemistry, Properties and Green Packaging Technology: A Review". *International Journal of Food Properties*, Vol. 14, No. 1, pp. 37-58, 2010.

[13] P. Krishnamachari, J. Zhang, J. Lou, J. Yan, and L. Uitenham "Biodegradable Poly(Lactic Acid)/Clay Nanocomposites by Melt Intercalation: A Study of Morphological, Thermal, and Mechanical Properties". *International Journal of Polymer Analysis and Characterization*, Vol. 14, No. 4, pp. 336-50, 2009.

[14] E. T. Thostenson, S. Ziaee, and T.-W. Chou "Processing and electrical properties of carbon nanotube/vinyl ester nanocomposites". *Composites Science and Technology*, Vol. 69, No. 6, pp. 801-04, 2009.

[15] J. Rhim, S. Hong, and C. Ha "Tensile, water vapor barrier and antimicrobial properties of PLA/nanoclay composite films". *LWT - Food Science and Technology*, Vol. 42, No. 2, pp. 612-17, 2009.

[16] A. Yamada, F. Niikura, and K. Ikuta "A three-dimensional microfabrication system for biodegradable polymers with high resolution and biocompatibility". *Journal of Micromechanics and Microengineering*, Vol. 18, No. 2, p. 025035, 2008.

[17] S. M. Berry, S. P. Warren, D. A. Hilgart, A. T. Schworer, S. Pabba, A. S. Gobin, R. W. Cohn, and R. S. Keynton "Endothelial cell scaffolds generated by 3D direct writing of biodegradable polymer microfibers". *Biomaterials*, Vol. 32, No. 7, pp. 1872-79, 2011.

[18] G. Vozzi, C. Flaim, A. Ahluwalia, and S. Bhatia "Fabrication of PLGA scaffolds using soft lithography and microsyringe deposition". *Biomaterials*, Vol. 24, No. 14, pp. 2533-40, 2003.

[19] J. Bruneaux, D. Therriault, and M. C. Heuzey "Micro-extrusion of organic inks for direct-write assembly". *Journal of Micromechanics and Microengineering*, Vol. 18, No. 11, p. 115020, 2008.

[20] G. D. Liang, S. P. Bao, and S. C. Tjong "Microstructure and properties of polypropylene composites filled with silver and carbon nanotube nanoparticles prepared by melt-compounding". *Materials Science and Engineering: B*, Vol. 142, No. 2-3, pp. 55-61, 2007.

[21] S. G. Hatzikiriakos and K. B. Migler, "Polymer processing instabilities: Control and understanding," ed: CRC, 2005, p. 87.

[22] S. Sinha Ray and M. Okamoto "New Polylactide/Layered Silicate Nanocomposites, 6". *Macromolecular Materials and Engineering*, Vol. 288, No. 12, pp. 936-44, 2003.

[23] J. K. Jeszka, L. Pietrzak, M. Pluta, and G. Boiteux "Dielectric properties of polylactides and their nanocomposites with montmorillonite". *Journal of*

Non-Crystalline Solids, Vol. 356, No. 11-17, pp. 818-21, 2010.
[24] E. Laredo, M. Grimau, A. Bello, D. F. Wu, Y. S. Zhang, and D. P. Lin "AC Conductivity of Selectively Located Carbon Nanotubes in Poly(ε-caprolactone)/Polylactide Blend Nanocomposites". *Biomacromolecules,* Vol. 11, No. 5, pp. 1339-47, 2010.
[25] Z. Gou and A. J. McHugh "Two-dimensional modeling of dry spinning of polymer fibers". *Journal of Non-Newtonian Fluid Mechanics,* Vol. 118, No. 2–3, pp. 121-36, 2004.
[26] Z. Gou and A. J. McHugh "A comparison of Newtonian and viscoelastic constitutive models for dry spinning of polymer fibers". *Journal of Applied Polymer Science,* Vol. 87, No. 13, pp. 2136-45, 2003.
[27] G. Deng, Q. Xia, Y. Xu, and Q. Zhang "Simulation of dry-spinning process of polyimide fibers". *Journal of Applied Polymer Science,* Vol. 113, No. 5, pp. 3059-67, 2009.
[28] N. Kojić, A. Kojić, and M. Kojić "Numerical determination of the solvent diffusion coefficient in a concentrated polymer solution". *Communications in Numerical Methods in Engineering,* Vol. 22, No. 9, pp. 1003-13, 2006.
[29] A. Rybak, G. Boiteux, F. Melis, and G. Seytre "Conductive polymer composites based on metallic nanofiller as smart materials for current limiting devices". *Composites Science and Technology,* Vol. 70, No. 2, pp. 410-16, 2010.
[30] A. Lonjon, L. Laffont, P. Demont, E. Dantras, and C. Lacabanne "New Highly Conductive Nickel Nanowire-Filled P(VDF-TrFE) Copolymer Nanocomposites: Elaboration and Structural Study". *The Journal of Physical Chemistry C,* Vol. 113, No. 28, pp. 12002-06, 2009.